

Rising droplets in a centrifugal field: A way to avoid interfacial contamination in liquid-liquid flow

Hassan El Itawi,^{1,2} Benjamin Lalanne^{1,*}, Subhadarshinee Sahoo², Emmanuel Cid¹,
Gladys Massiera², Nathalie Le Sauze,¹ and Olivier Masbernat¹

¹Laboratoire de Génie Chimique, Université de Toulouse, CNRS, INPT, UPS, Toulouse, France

²Laboratoire Charles Coulomb, Université de Montpellier, CNRS, Montpellier, France



(Received 6 November 2023; accepted 21 March 2024; published 3 May 2024)

Investigations of the settling of liquid droplets in another liquid phase have to deal with the potential contamination of the interfaces with residual impurities. It is shown in this Letter that the use of a centrifugal field to generate the drop settling may overcome this issue: the drop terminal velocity and shape are reached at much shorter time scales than that taken by contaminant adsorption from the bulk to the interface, so it is possible to obtain data for clean interfaces. In this study, using a centrifuged cell, drop formation, velocity, and shape have been characterized in the inertial regime. By comparing these quantities to theoretical models and by performing complementary direct numerical simulations with clean interfaces, it is proved that interfacial contamination can be disregarded in the experiments. Such an experiment can therefore be used to establish results of reference for clean interfaces. For instance, a correlation for the drop deformation of settling droplets in clean liquid-liquid systems is obtained for a wide range of parameters, as a function of the sole Weber number. It emphasizes that clean droplets are less distorted than clean bubbles.

DOI: [10.1103/PhysRevFluids.9.L051601](https://doi.org/10.1103/PhysRevFluids.9.L051601)

In multiphase flows, it has been known for a long time that the presence of impurities or surfactants strongly affects the hydrodynamics [1]. Indeed, they generate Marangoni stresses in case of surface tension gradients along an interface, which produce surface flows [2], and possibly confer surface viscoelasticity in case of a complex interfacial film [3,4]. Even a very small uncontrolled concentration of adsorbed molecules may have significant effects on the interface dynamics [5]. Such a condition occurs in case of residual contamination of any of the bulk fluids (presence of impurities), which is hardly avoidable. The interfacial tension can still be very close to that of a clean interface [17], but the existence of Marangoni stresses generates drastic consequences on the hydrodynamics. Such effects include a decrease of the terminal velocity of bubbles or droplets [1,6], a strong increase in the damping rate of interfacial capillary waves [7] or shape oscillations [8,9], a significant decrease of mass transfer rates around bubbles [10] due to adsorbed surfactants, or, conversely, the enhancement of mass transfer rate around droplets due to Marangoni stress-induced interfacial turbulence [11,12]. Also, interdrop film drainage is very sensitive to surface contamination [13], Marangoni stresses induce subsequent impact on the thickness of the coating of a solid when it is removed from a liquid bath (Landau-Levich problem [14]) or on the lifetime of bubbles [15] at a free surface. However, the concentration of contaminants at an interface is still challenging to evaluate [16,17].

The strong impact of Marangoni stresses highlights the need of having reference cases of flows around clean interfaces. Nevertheless, impurities are ubiquitous and rapidly adsorb at the

*Corresponding author: benjamin.lalanne@ensiacet.fr

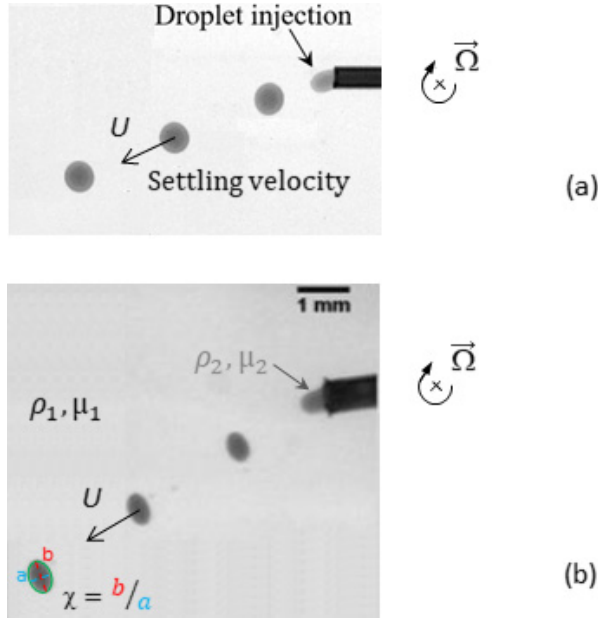


FIG. 1. Drop formation and settling in the rotating cell, for (a) a nearly spherical and (b) an ellipsoidal droplet.

interfaces, in particular in liquid-liquid dispersions because they can be present in both phases. As a consequence, in most studies, the settling velocity of liquid droplets in another liquid matches the theoretical value assuming no slip for the fluid at the interface, referred to as a case of immobile interface, as for a solid particle [18]. For instance, the experimental verification of Hadamard-Rybczynski drag law for liquid droplets requires an extensive and tedious cleaning procedure of the experimental device and phase systems, which cannot be achieved in a routine protocol [19]. In this Letter, an alternative method is proposed to form and study droplets which behave as contaminant free. It is based on the use of a centrifugal field and very short time experiments. Indeed, whereas the time scales associated to the transfer of impurities or surfactants from the bulk to the interface cannot be easily monitored, the time scales of the drop formation and motion can be reduced by increasing the gravitational acceleration, using centrifugation for instance. The aim of this Letter is to show that this experimental method allows to investigate the dynamics of a liquid drop in another liquid with a contaminant-free interface.

The experimental device is composed of two cells of the same mass, connected by a capillary: a reservoir cell filled with phase 2 (drop phase) and an injection cell containing the continuous phase 1 (see Appendix A [20] for more details about the device and image processing). The assembly is fixed inside the bowl of a spin coater which can provide centrifugal accelerations ranging between 20 and 2400g (g being the acceleration of gravity) due to the rotation speed. A pressure regulator sends an overpressure of air to the reservoir cell that produces a flow of phase 2 toward the injection cell: the injection of a drop of phase 2 in phase 1 can thereby be generated in a dripping regime, as shown in Figs. 1(a) and 1(b). Several experimental conditions, E_{1-25} , have been tested, varying the density contrast ($\rho_2 - \rho_1$), the angular rotation speed ω , the surface tension γ_{12} , or the capillary diameter D_i (Table 1 in Appendix B [20]). Phase 1 is a silicon oil of variable chain length in order to explore a range of density ρ_1 and viscosity μ_1 ; phase 2 is a 25% w/w aqueous solution of sucrose.

In the injection cell, the settling of the droplet is recorded by a high-speed camera (a LED panel is used as the light source), synchronized with the passage of the cell. Images of the observation

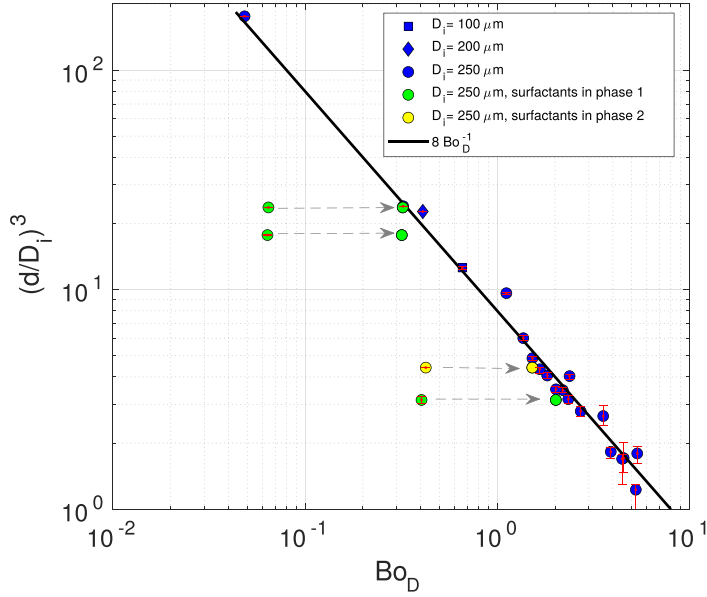


FIG. 2. Scaling law, Eq. (1), and experimental points [20] for the drop size at detachment; the four arrows shift the Bo_D of cases E_{21-24} , containing surfactants, by considering the same surface tension as for a clean interface.

window are taken at a rate of 9295 frames per second with a spatial resolution of 512×512 pixels, achieving a good compromise between the frequency of images captured and their resolution.

Through an analysis of the drop detachment condition in this device, rising velocity, and deformation, we demonstrate that the droplet interfaces behave as contaminant-free interfaces.

First, regarding the injection stage through a capillary of internal diameter D_i , the drop diameter d varies between $230 \mu\text{m}$ and 1.4 mm , with a standard deviation between 5 and $12 \mu\text{m}$ for all cases (up to 350 droplets are formed for each condition). During the drop formation process, the interface deformation is controlled by interfacial stresses rather than internal viscous stresses, since the Ohnesorge number $Oh_D = \mu_2 / \sqrt{\rho_2 \gamma_{12} D_i}$ is of order of 10^{-2} (ρ_2 and μ_2 being the drop density and viscosity, respectively). Therefore, the drop detachment is expected to be given by the balance between the centrifugal force $(\rho_2 - \rho_1) \omega^2 r_0 \pi d^3 / 6$ (r_0 is the distance from the capillary tip to the rotation axis) and the capillary force $\alpha \pi \gamma_{12} D_i$, with α a coefficient accounting for wettability effects and the influence of tip roughness. Such force balance predicts a drop diameter at detachment evolving as $(d/D_i)^3 = 6\alpha / Bo_D$, with $Bo_D = (\rho_2 - \rho_1) \omega^2 r_0 D_i^2 / \gamma_{12}$ the Bond number. Figure 2 shows that this quasistatic balance is relevant to predict the drop size in this experiment, even for values of the Reynolds number in the capillary, Re_D (based on D_i , properties of phase 2 and the velocity in the capillary), up to 25. Indeed, the different experimental conditions nicely collapse in the master curve of Fig. 2, leading to

$$\left(\frac{d}{D_i}\right)^3 = \frac{8}{Bo_D}. \quad (1)$$

Equation (1) is consistent with the results of Zhang *et al.* [21], who found that the drop size was weakly affected by the viscosity ratio $\lambda_{12} = \mu_2 / \mu_1$.

In Fig. 2, four points correspond to conditions (E_{21-24}) where surfactants have been added at concentrations above the critical micelle concentration (CMC), either in phase 1 (ethoxylated silicone copolymer, DBE), or in phase 2 (sodium lauryl sulfate, SDS). Note that the resulting droplets have a diameter which is very close to that obtained in the absence of surfactants (d is

smaller than 4%). Yet, if the adsorption equilibrium was reached, these surfactants should have reduced the surface tension by at least a factor of 3.5 (from 40 to 8 mN/m with DBE, and from 43 to 12 mN/m with SDS), which should therefore have decreased the drop size as per Eq. (1). As shown in Fig. 2, when the surface tension at equilibrium is used in Bo_D , these four points are completely out of the general trend scaling the drop size at detachment. However, using the value of γ_{12} for clean interfaces in Bo_D shifts their abscissas, and makes them follow the master curve. This suggests that the interfaces of these droplets are not covered with surfactants, with a γ_{12} value still far from equilibrium. Such a result can be interpreted by comparing the time of drop formation t_f , to the time t_s of surfactant transfer from the bulk toward the newly created interface (like in the study of drop formation in microchannels by Kalli *et al.* [22]), by reasonably assuming that there is no adsorption barrier. As detailed in Appendix C [20] (including Refs. [23–27]), $t_s \sim D/k_L^2$ is estimated as the diffusion time (with D the diffusion coefficient of the surfactant in the bulk) over the mass boundary layer thickness around the interface (k_L being the mass transfer coefficient, computed from a relevant correlation depending if the surfactant is in phase 1 or 2). Here, it results that $t_s \gg t_f$: the drop is formed 20 to 100 faster than the characteristic time of surfactant diffusion, this factor being much larger (of about 700) when the surfactant is inside the drop (these figures have been estimated with a surfactant concentration above the CMC). These figures explain that the presence of surfactants at the drop surface can be neglected during its formation, leading to a γ_{12} value close to that for a clean interface. Obviously, such a conclusion applies even more when considering contaminants only present at very small concentration (compared to the CMC) or traces, in any of the liquid phases.

Second, based on experimental conditions without surfactants, we evaluate the presence of contaminant traces at the drop surface by comparing the drop velocity and shape to theoretical predictions. Indeed, these quantities are strongly sensitive to the interface contamination. Predictions from both a force balance model and direct numerical simulations (DNS) are used. The analysis is carried out on cases E_{25} , E_{16} , E_5 , and E_{14} (Table 1 [20]).

In these experiments, the distance between two consecutive droplets lies between six and eight drop diameters d , and a velocity plateau is reached after short travel distances of a few d . By using DNS of both isolated droplets and droplets within a train (periodic boundary conditions), we have verified that the rising dynamics of one drop is not affected by the wake of its neighbors over very short times (see Appendix D [20], including Ref. [28]), for these distances between consecutive droplets. The following comparison with models for isolated droplets is therefore relevant.

The force balance equation includes both the centrifugal and Coriolis forces. It is written on one droplet in polar coordinates (r, θ) , from the frame rotating with the injection cell (the third axis of the frame is aligned with the rotation vector $\vec{\Omega}$):

$$\begin{aligned} m \left(\frac{d^2 r}{dt^2} - r \left[\frac{d\theta}{dt} \right]^2 \right) &= (\rho_2 - \rho_1) V_d r \Omega^2 + 2\rho_2 V_d \Omega r \frac{d\theta}{dt} - \frac{1}{2} \rho_1 C_D S_p U \frac{dr}{dt} \\ m \left(r \frac{d^2 \theta}{dt^2} + 2 \frac{dr}{dt} \frac{d\theta}{dt} \right) &= -2\rho_2 V_d \Omega \frac{dr}{dt} - \frac{1}{2} \rho_1 C_D S_p U r \frac{d\theta}{dt}. \end{aligned} \quad (2)$$

V_d is the drop volume, $m = V_d(\rho_2 + C_M(\chi)\rho_1)$ the drop and added mass, $S_p = \pi R^2$ the projected surface area, and $U = \sqrt{(dr/dt)^2 + (rd\theta/dt)^2}$ the magnitude of the relative velocity between the drop and the external liquid in the rotating frame. The added-mass coefficient C_M depends on the drop aspect ratio χ (experimentally known) based on the expression of Rastello *et al.* [29] ($0.5 \leq C_M \leq 0.95$ for cases of Fig. 3). As there is no general correlation for the drag coefficient C_D for deformed drops, expressions for a sphere are considered in two contrasted cases: (i) a mobile (clean) interface, using the correlation from Rivkind and Ryskin [30]; and (ii) a fully immobile (contaminated) interface, computing C_D from Schiller and Naumann's [31] correlation (as for a solid particle). Equation (2) is solved by taking the initial drop velocity and position from the experimental data. Figure 3 compares the model prediction to the experimental results of the

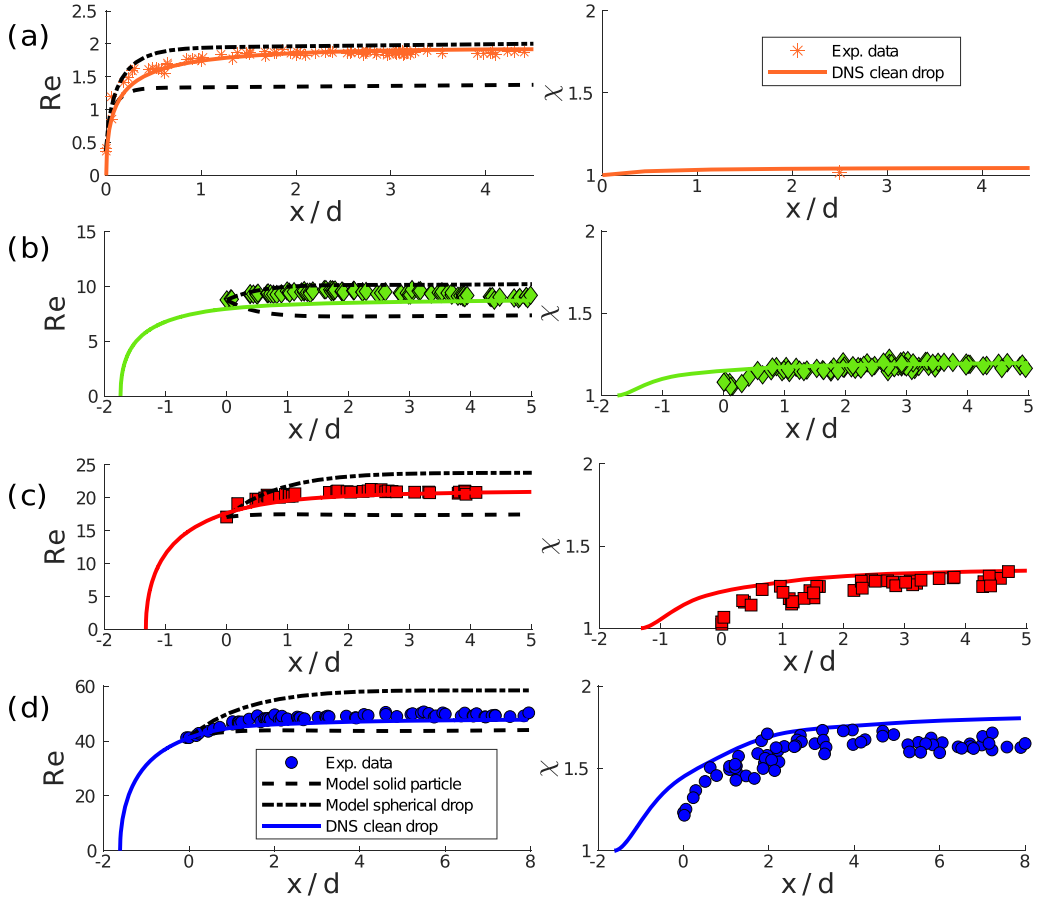


FIG. 3. Cases [20] (a) E_{25} , (b) E_{16} , (c) E_5 , and (d) E_{14} . Evolution of the Reynolds number Re and aspect ratio χ as a function of the distance traveled by the droplet in the experiments, compared to the predictions from the force balance model of Eq. (2), and DNS results without surfactants.

evolution of the droplet Reynolds number $Re = \rho_1 U d / \mu_1$ as a function of the normalized traveled distance, denoted as x/d . The velocity of case E_{25} , where the drop is undistorted, matches the prediction for a clean spherical droplet. In cases E_{16} , E_5 , E_{14} involving deformed droplets, the terminal velocity measured lies between the theoretical curves corresponding to mobile (i) and immobile (ii) interfaces of spherical drops. Two effects could explain the discrepancy: either a contamination of the interface or the drop deformation. However, since the experimental velocity consistently exceeds that of a solid particle, the interfaces are not fully immobile.

To go deeper in the analysis, DNS of the Navier-Stokes equations have been carried out, solved with the one-fluid approach by the *DIVA* [32] code. The deformable drop is captured by the level-set method on a fixed grid of 48 nodes per radius, such a resolution allowing to accurately compute the drop dynamics in this range of Reynolds numbers [33,34]. The simulations are axisymmetric and solve the motion after the drop detachment (by using the experimental radius and drop position at release) in a rotating frame centered on the droplet center of mass, with the same approach as in El Itawi *et al.* [34] (details are given in this reference): the centrifugal force is considered, but the Coriolis force is neglected. This choice is practical to remain under the axisymmetric assumption, and is justified because the velocity drift induced by the Coriolis force is small compared to that induced by the centrifugal acceleration. In the simulations, conditions of a clean interface are

assumed: γ_{12} takes the value of a clean interface, and no Marangoni effect is considered, i.e., the tangential stresses are continuous at the interface. In Fig. 3, the evolution of both the instantaneous drop Reynolds number and aspect ratio, χ , defined as the major-to-minor axis length ratio, are compared against experimental results. Some initial conditions differ in the simulations: the drop is initially spherical with zero velocity. The comparison is therefore relevant when initial conditions are forgotten, i.e., after a travel distance of one or two d . For all cases, a very good match is obtained between the experimental and numerical evolution of the velocity. Concerning χ , the experimental data are slightly scattered, but the agreement with the DNS is very good for E_{25} , E_{16} , E_5 , and the experimental drop E_{14} is only slightly less deformed (of less than 10%) compared to the simulation. Thus, DNS without surfactants accurately reproduce the experimental measurements of both the rise velocity and drop distortion: it proves that if the velocity is smaller than that of a clean spherical drop, it is due to its oblate shape and not due to any contamination. Such comparison confirms that these droplets behave as contaminant free in this experiment. This means that the centrifugal field allows to reach a steady state regime for the drop dynamics in a much shorter time than that taken by the contaminants to diffuse from the bulk to the interface (which is a low rate transfer process). The short residence times due to centrifugation make this requirement possible, even with small density difference and drop size.

Experimentally, note that the clean interface condition is easier to satisfy at larger acceleration, for a droplet of given size. Indeed, the impact of contaminants on the drop velocity is related to the stagnant-cap angle θ_{cap} [1,35], resulting from the contaminant accumulation at the rear of the drop during its rise. θ_{cap} will not be the same depending on the loading of the interface [9,35]. The larger the drop velocity, the smaller its travel time, the smaller the surface contamination. As a result, the drag coefficient will be closer to that of a clean droplet at larger velocity, on the basis of DNS results about θ_{cap} from Kentheswaran *et al.* [10] (see their Fig. 6). This interpretation suggests that the contaminant-free condition is more difficult to obtain at smaller Reynolds number.

Regarding our experimental conditions where surfactants were included in one of the bulk phases, the concentrations are high (above the CMC), preventing the clean interface condition from being reached. Indeed, for case E_{22} with SDS inside the drop, and case E_{21} with DBE in the continuous phase, the experimental velocity matches that predicted by the force balance model for immobile interfaces; see Appendix E [20] (including Refs. [1,9,10,26,35–38]). For such high surfactant concentration, the flux of surfactants toward the interface is larger, and enough to develop a Marangoni stress that immobilizes the interface. Yet, the surface tension is close to that of a clean system (Fig. 2) at the moment of drop detachment. It is therefore observed that the rising dynamics of a droplet is more sensitive to Marangoni stresses than the drop formation process.

Finally, the use of centrifugation has been shown to be valuable to analyze the dynamics of interfaces without adsorbed impurities (cases of Fig. 3). This conclusion has been obtained with drop sizes of a few hundreds of micrometers, leading to Reynolds numbers between 1 and 50, and over a few milliseconds of residence time.

Third, the experimental drop shapes are compared to existing results. However, there was no general relationship able to predict the aspect ratio χ for clean liquid-liquid systems [18,39]. In order to fill this gap, data have been collected from numerical simulations of Bäumlér *et al.* [40] and Albert *et al.* [41]. Additional DNS of clean rising droplets have also been performed with the *DIVA* code (see Table 3 in Appendix F [20]). The data set has density ratios of the order of unity, but covers a wide range of both viscosity ratios ($0.25 \leq \lambda_{12} \leq 45$), Reynolds, and Bond numbers, in the inertial regime. Only stable axisymmetric results are considered, for which the drop shape can be accurately described by an ellipsoid, and below the threshold for which a bifurcation toward a three-dimensional dynamics appears [44] (this bifurcation is mentioned in the quoted references [40–43], identified through comparisons to experimental data or 3D simulations). In Fig. 4, all these numerical results on droplets collapse on a master curve describing the evolution of χ as a function of the sole Weber number $We = \rho_1 U^2 d / \gamma_{12}$, which quantifies the inertial-to-surface

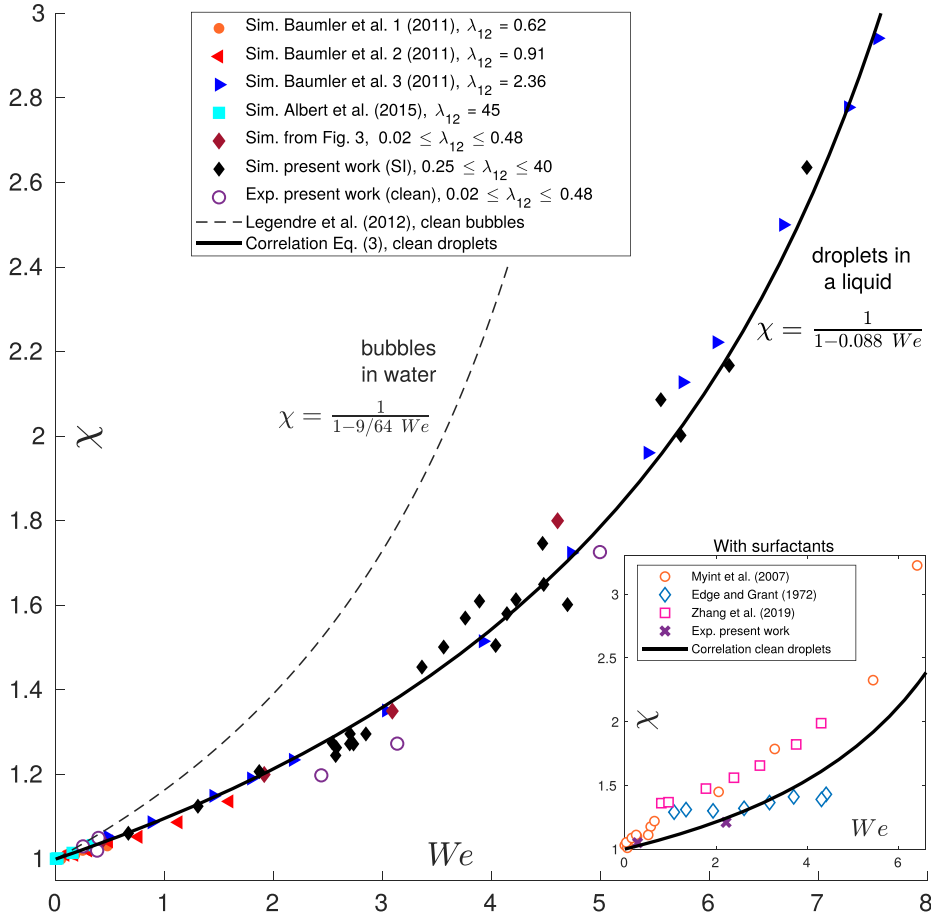


FIG. 4. Drop aspect ratio χ versus We : several numerical [20,40,41] and experimental results [20] (without surfactants), compared to the correlation proposed, Eq. (3), for clean liquid-liquid droplets. Inset: same plot including experiments with surfactants at large concentration (cases E_{21-22} [20]) and previous experimental results [47–49].

tension forces ratio at the scale of the drop. The following correlation is obtained:

$$\chi = \frac{1}{1 - 0.088 We}. \quad (3)$$

Figure 4 shows that Eq. (3) is satisfied for a large variety of clean droplets, under stable axisymmetric regimes. It emphasizes that liquid-liquid droplets are less distorted than bubbles (in that case, coefficient before We is $9/64$ [45]). Indeed, as mentioned by Hinze [46], the internal viscosity of these droplets dissipates energy from the rising motion, which mitigates their distortion. Based on Fig. 4, the present experimental data involving clean droplets (Table 2 in the SM [20]) are also fully consistent with this correlation: they follow the trend of Eq. (3) well, with maximum deviation of 8%. Note that Eq. (3) does not directly involve λ_{12} (Myint *et al.* [47] pointed out that λ_{12} does not affect much χ but rather the drop fore-and-aft symmetry).

Then, it is interesting to evaluate the effect of surfactants on the deformation. In the inset of Fig. 4, our two experimental cases E_{21-22} with surfactants at concentration above the CMC are included (cross symbols), for which the drop velocities match those of solid particles. A good agreement of χ is also obtained with the proposed correlation, which leads to showing that the drop aspect

ratio is less sensitive to interface contamination than the rise velocity. Other experimental results with surfactant-covered droplets [47–49] are plotted in the inset of Fig. 4: a significant scatter is observed, with contrasted behavior, either above, on, or below the reference curve. At this stage, no precise conclusion can thus be derived about the impact of surfactants on χ , because it probably depends on both the actual coverage of the interface, the intensity of the Marangoni stresses [50] or more complex interfacial forces. Such a question needs to be addressed in a dedicated investigation through experiments where surfactant adsorption has time to reach steady state.

Finally, the use of the centrifugal force has proven to be a relevant means for studying the dynamics of contaminant-free droplets over short times, in the absence of surfactants. Such an experiment is therefore promising to establish benchmark results on droplet dynamics in the absence of Marangoni stresses, like the general trend on droplet deformation exhibited in Fig. 4, or the investigation of other problems such as interdroplet coalescence.

The authors gratefully acknowledge the French Research National Agency (ANR) for financial support through the program “Encapsulation Process by Droplet Interface Crossing” (project reference: ANR-15-CE08-0026).

-
- [1] V. G. Levich, *Physicochemical Hydrodynamics* (Prentice-Hall, Englewood Cliffs, 1962).
 - [2] J. P. Chevaillier, E. Klaseboer, O. Masbernat, and C. Gourdon, Effect of mass transfer on the film drainage between colliding drops, *J. Colloid Interface Sci.* **299**, 472 (2006).
 - [3] T. Verwijlen, L. Imperiali, and J. Vermant, Separating viscoelastic and compressibility contributions in pressure-area isotherm measurements, *Adv. Colloid Interface Sci.* **206**, 428 (2014).
 - [4] P. Bazazi, H. A. Stone, and S. H. Hejazi, Dynamics of droplet pinch-off at emulsified oil-water interfaces: Interplay between interfacial viscoelasticity and capillary forces, *Phys. Rev. Lett.* **130**, 034001 (2023).
 - [5] H. Manikantan and T. M. Squires, Surfactant dynamics: hidden variables controlling fluid flows, *J. Fluid Mech.* **892**, P1 (2020).
 - [6] S. Takagi and Y. Matsumoto, Surfactant effects on bubble motion and bubbly flows, *Annu. Rev. Fluid Mech.* **43**, 615 (2011).
 - [7] J. Saylor, A. Szeri, and G. Foulks, Measurement of surfactant properties using a circular capillary wave field, *Exp. Fluids* **29**, 509 (2000).
 - [8] H. L. Lu and R. Apfel, Shape oscillations of drops in the presence of surfactants, *J. Fluid Mech.* **222**, 351 (1991).
 - [9] A. Piedfert, B. Lalanne, O. Masbernat, and F. Risso, Numerical simulations of a rising drop with shape oscillations in the presence of surfactants, *Phys. Rev. Fluids* **3**, 103605 (2018).
 - [10] K. Kentheswaran, N. Dietrich, S. Tanguy, and B. Lalanne, Direct numerical simulation of gas-liquid mass transfer around a spherical contaminated bubble in the stagnant-cap regime, *Int. J. Heat Mass Transf.* **198**, 123325 (2022).
 - [11] C. A. Sternling and L. E. Scriven, Interfacial turbulence: hydrodynamic instability and the Marangoni effect, *AIChE J.* **5**, 514 (1959).
 - [12] M. Wegener, J. Grünig, J. Stüber, A. R. Paschedag, and M. Kraume, Transient rise velocity and mass transfer of a single drop with interfacial instabilities—experimental investigations, *Chem. Eng. Sci.* **62**, 2967 (2007).
 - [13] H. Shen and S. Hartland, Effect of interfacial concentration gradients of insoluble surfactants on local film-thinning, *J. Colloid Interface Sci.* **167**, 94 (1994).
 - [14] D. Quéré, Fluid coating on a fiber, *Annu. Rev. Fluid Mech.* **31**, 347 (1999).
 - [15] O. Atasi, D. Legendre, B. Haut, R. Zenit, and B. Scheid, Lifetime of surface bubbles in surfactant solutions, *Langmuir* **36**, 7749 (2020).

- [16] S. Hosokawa, Y. Masukura, K. Hayashi, and A. Tomiyama, Experimental evaluation of Marangoni stress and surfactant concentration at interface of contaminated single spherical drop using spatiotemporal filter velocimetry, *Int. J. Multiphase Flow* **97**, 157 (2017).
- [17] B. Lalanne, O. Masbernat, and F. Risso, Determination of interfacial concentration of a contaminated droplet from shape oscillation damping, *Phys. Rev. Lett.* **124**, 194501 (2020).
- [18] R. Clift, J. R. Grace, and W. E. Weber, *Bubbles, Drops, and Particles* (Courier Corporation, Chelmsford, MA, 2005).
- [19] M. Mahe, M. Vignes-Adler, A. Rousseau, C. G. Jacquin, and P. M. Adler, Adhesion of droplets on a solid wall and detachment by a shear flow: I. Pure systems, *J. Colloid Interface Sci.* **126**, 314 (1988).
- [20] See Supplemental Material at <http://link.aps.org/supplemental/10.1103/PhysRevFluids.9.L051601> for explanations about the experimental device (Appendix A), the detail of all experimental conditions (Appendix B), time scale estimations regarding the mass transfer of surfactants (Appendix C), simulations that compare the dynamics of an isolated droplet and a droplet within a train (Appendix D), an example of rise velocity for a condition where surfactants have been included (Appendix E), and the parameters of the additional DNS of drop rise in another liquid with a clean interface (Appendix F).
- [21] D. F. Zhang and H. A. Stone, Drop formation in viscous flows at a vertical capillary tube, *Phys. Fluids* **9**, 2234 (1997).
- [22] M. Kalli, L. Chagot, and P. Angeli, Comparison of surfactant mass transfer with drop formation times from dynamic interfacial tension measurements in microchannels, *J. Colloid Interface Sci.* **605**, 204 (2022).
- [23] H. Ma and J. Xu, Mean-Square Radius of Gyration of Poly(dimethylsiloxane) Chain with Side Groups, *Polymer J.* **26**, 779 (1994).
- [24] W. E. Ranz and W. R. Marshall, Evaporation from drops, *Chem. Engng. Prog.* **48**, 141 (1952).
- [25] A. C. Ribeiro, V. M. Lobo, E. F. Azevedo, M. D. G. Miguel, and H. D. Burrows, Diffusion coefficients of sodium dodecylsulfate in aqueous solutions of sucrose and in aqueous solutions, *J. Mol. Liq.* **94**, 193 (2001).
- [26] D. Colombet, D. Legendre, A. Cockx, and P. Guiraud, Mass or heat transfer inside a spherical gas bubble at low to moderate Reynolds number, *Int. J. Heat Mass Transf.* **67**, 1096 (2013).
- [27] A. Rachih, D. Legendre, E. Climent, and S. Charton, Numerical study of conjugate mass transfer from a spherical droplet at moderate Reynolds number, *Int. J. Heat Mass Transf.* **157**, 119958 (2020).
- [28] H. Yuan and A. Prosperetti, On the in-line motion of two spherical bubbles in a viscous fluid, *J. Fluid Mech.* **278**, 325 (1994).
- [29] M. Rastello, J.-L. Marié, and M. Lance, Drag and lift forces on clean spherical and ellipsoidal bubbles in a solid-body rotating flow, *J. Fluid Mech.* **682**, 434 (2011).
- [30] V. Rivkind and G. Ryskin, Flow structure in motion of a spherical drop in a fluid medium at intermediate Reynolds numbers, *Fluid Dyn.* **11**, 5 (1976).
- [31] L. Schiller and A. Naumann, A drag coefficient correlation, *Z. Verein. Deutsch. Ing.* **77**, 318 (1935).
- [32] B. Lalanne, L. Rueda-Villegas, S. Tanguy, and F. Risso, On the computation of viscous terms for incompressible two-phase flows with Level Set/Ghost Fluid Method, *J. Comput. Phys.* **301**, 289 (2015).
- [33] B. Lalanne, S. Tanguy, and F. F. Risso, Effect of rising motion on the damped shape oscillations of drops and bubbles, *Phys. Fluids* **25**, 112107 (2013).
- [34] H. El Itawi, B. Lalanne, G. Massiera, N. Le Sauze, and O. Masbernat, Numerical simulation of the crossing of a liquid-liquid interface by a droplet, *Phys. Rev. Fluids* **5**, 093601 (2020).
- [35] S. S. Sadhal and R. E. Johnson, Stokes flow past bubbles and drops partially coated with thin films. Part 1. Stagnant cap of surfactant film—exact solution, *J. Fluid Mech.* **126**, 237 (1983).
- [36] N. Kishore and S. Gu, Momentum and heat transfer phenomena of spheroid particles at moderate Reynolds and Prandtl numbers, *Int. J. Heat Mass Transf.* **54**, 2595 (2011).
- [37] A. Weiner, C. M. Claassen, I. R. Hierck, J. A. M. Kuipers, and M. W. Baltussen, Assessment of a subgrid-scale model for convection-dominated mass transfer for initial transient rise of a bubble, *AIChE J.* **68**, e17641 (2022).
- [38] P. Albrand and B. Lalanne, Mass transfer rate in gas-liquid Taylor flow: Sherwood numbers from numerical simulations, *Chem. Eng. Sci.* **280**, 119011 (2023).

- [39] M. Wegener, M. Kraume, and A. R. Paschedag, Terminal and transient drop rise velocity of single toluene droplets in water, *AIChE J.* **56**, 2 (2010).
- [40] K. Bäumlner, M. Wegener, A. R. Paschedag, and E. Bänsch, Drop rise velocities and fluid dynamic behavior in standard test systems for liquid/liquid extraction—experimental and numerical investigations, *Chem. Eng. Sci.* **66**, 426 (2011).
- [41] C. Albert, J. Kromer, A. M. Robertson, and D. Bothe, Dynamic behaviour of buoyant high viscosity droplets rising in a quiescent liquid, *J. Fluid Mech.* **778**, 485 (2015).
- [42] R. F. Engberg and E. Y. Kenig, An investigation of the influence of initial deformation on fluid dynamics of toluene droplets in water, *Int. J. Multiphase Flow* **76**, 144 (2015).
- [43] A. H. Charin, P. L. Lage, L. F. L. Silva, Ž. Tuković, and H. Jasak, On the dynamic behavior of rising droplets, *Int. J. Multiphase Flow* **110**, 165 (2019).
- [44] H. Godé, Modélisation et simulation des écoulements et du transfert de matière autour d'une goutte sphérique: de l'analyse locale à de nouveaux modèles, Ph.D. Thesis, Toulouse INP (2023).
- [45] D. Legendre, R. Zenit, and J. Rodrigo Velez-Cordero, On the deformation of gas bubbles in liquids, *Phys. Fluids* **24**, 043303 (2012).
- [46] J. O. Hinze, Fundamentals of the hydrodynamic mechanism of splitting in dispersion processes, *AIChE J.* **1**, 289 (1955).
- [47] W. Myint, S. Hosokawa, and A. Tomiyama, Shapes of single drops rising through stagnant liquids, *J. Fluid Sci. Tech.* **2**, 184 (2007).
- [48] R. M. Edge and C. D. Grant, The motion of drops in water contaminated with a surface-active agent. *Chem. Eng. Sci.* **27**, 1709 (1972).
- [49] J. Zhang, Y. Wang, G. W. Stevens, and W. Fei, An experimental study on single drop rising in a low interfacial tension liquid–liquid system, *Chem. Eng. Res. Design* **148**, 349 (2019).
- [50] K. Kentheswaran, W. Antier, N. Dietrich, and B. Lalanne, Impact of surfactants on the rise of deformable bubbles and interfacial gas-liquid mass transfer, *J. Fluid Mech.* **970**, A5 (2023).